Journal of Magnetism and Magnetic Materials 529 (2021) 167860

Contents lists available at ScienceDirect

Journal of Magnetism and Magnetic Materials

journal homepage: www.elsevier.com/locate/jmmm

# Ferromagnetic resonance study on the influence of the electrolytic bath acidity on the magnetic anisotropy of Ni nanowires

Jonathan Almazán-Celis [a], Luis E. Díaz-Sánchez [a], Oscar F. Olea-Mejía [b], Luc Piraux [c], Joaquín de la Torre Medina [d,*]

[a] Facultad de Ciencias, Universidad Autónoma del Estado de México, Instituto Literario No. 100. C. P. 50000 Toluca, Mexico
[b] Facultad de Química, Universidad Autónoma del Estado de México, Instituto Literario No. 100. C. P. 50000 Toluca, Mexico
[c] Institute of Condensed Matter and Nanosciences, Université catholique de Louvain. Place Croix du Sud 1, B-1348, Louvain-la-Neuve, Belgium
[d] Instituto de Investigaciones en Materiales – Unidad Morelia, Universidad Nacional Autónoma de México. Antigua Carretera a Pátzcuaro No. 8701 Col. Ex Hacienda de San José de la Huerta, C. P. 58190, Morelia, Mexico

ARTICLE INFO

*Keywords:*
Ferromagnetic resonance
Magnetic anisotropy
Electrolytic bath acidity
Ni nanowires

ABSTRACT

In this work, a ferromagnetic resonance study on the influence of the electrolytic bath acidity on the magnetic anisotropy and hardness parameter of arrays of 50 nm diameter Ni nanowires in porous alumina membranes, is reported. Fine tuning the effective magnetic anisotropy of the arrays has been achieved by progressively changing the nanowires microstructure from polycrystalline textured to single-crystalline as the electrolyte acidity is reduced. The micro-structural analysis carried out by X-ray diffraction and high resolution transmission electron microscopy has revealed that a preferred crystal texture is not a sufficient condition for the enhancement of the magnetic anisotropy. Instead, a correlation between the increase of crystallite size and quality, and the increase of both the magnetic anisotropy and hardness parameter has been shown. Ferromagnetic resonance and alternating gradient magnetometry experiments have shown that no additional magnetic contributions take place in Ni NWs grown from highly acidic electrolytes (pH 1.6), whereas a significant additional anisotropy contribution progressively appears as the electrolyte acidity is reduced (pH 5.0). Besides the careful adjustment of electrodeposition conditions, achieving a very long length for the nanowires is also a key requirement to have a precise control on the effective magnetic anisotropy energy, which can be fine tuned in the wide range from 64 −167 kJ·m$^{-3}$ as a result of an energy enhancement of magnetoelastic origin. Ferromagnetic resonance measurements have demonstrated that nanocomposites based on arrays of nanowires made of low cost and abundant elements like Ni exhibit hardness parameters in the range 0.47–0.75 within the semihard region, where those with $\kappa > 0.5$ are suitable for permanent magnet applications. These features make arrays of low diameter Ni nanowires very appealing for their use in the development of agile microwave and spintronic devices.

## 1. Introduction

The quest for novel materials with improved magnetic properties and unusual effects is at the center of an intense research activity due to their promising applications in the fields of spintronics [1], spin-caloritronics [2], logic devices and reservoir computing [3–5], magnetic sensors [6,7] and microwave devices [8,9]. A well known strategy to obtain new materials with enhanced magnetic anisotropy is via alloying and doping of transition metals with other elements [10]. As a result of that strategy is the emergence of the well known tetragonal crystal structure of Fe and Co based alloys and rare earths based ferromagnets that is responsible of a large magnetocrystalline anisotropy energy of the order of $10^6$ to $10^7$ erg·cm$^{-3}$ which confers the magnetic hardness of those materials [11–13]. However, most of the elements used in the fabrication of semihard ($0.1 \leqslant \kappa \leqslant 1$) and hard ($\kappa > 1$) magnets, with $\kappa$ the hardness parameter, are neither low cost nor abundant on Earth [13–15]. Therefore, the development of magnets based on low cost and more abundant elements is at the center of an intense research activity [16]. Exploiting other sources of magnetism and effects in order to enhance the effective magnetic anisotropy is paramount for the development of rare-earth-free magnets [17–22]. Nickel is an abundant magnetic material with interesting properties like its high magnetostriction that can

* Corresponding author.
*E-mail address:* delatorre@iim.unam.mx (J. de la Torre Medina).

https://doi.org/10.1016/j.jmmm.2021.167860
Received 27 July 2020; Received in revised form 11 January 2021; Accepted 11 February 2021
Available online 4 March 2021

be used to modify its effective magnetic anisotropy [23] for developing voltage controlled applications [24]. On the other hand, permanent magnets can be fabricated using magnetic nanowire (NW) arrays based on the high shape anisotropy and orientation of the NW assemblies with high aspect ratio and high coercivity [25]. Besides, electrochemical synthesis in porous membranes as templates is a powerful method for fabricating multicomponent NWs with different metals due to its engineering simplicity, versatility, and low-cost [26]. The magnetic properties of Ni NWs are strongly influenced by the type of porous host matrix [27,28] and NWs parameters like their diameter, packing fraction and aspect ratio [29,30] and electrodeposition parameters [31]. As shown in previous works, a very significant source of magnetic anisotropy in magnetic NWs can be obtained by magnetoelastic (ME) effects induced by thermally induced mechanical stresses [27,32–34]. However, this additional anisotropy contribution can not be exploited for practical applications as it is induced at low temperature as a result of the expansion coefficient mismatch between the NWs and the host polycarbonate porous membrane. In order to overcome this limitation it has been recently shown that ME effects can be induced at room temperature in arrays of very long Ni NWs embedded in anodic aluminum oxide (AAO) porous membranes [35]. For these materials, the combination of a preferred crystal texture along the [110] direction and confinement of the NWs diameter to some tenths of nanometers is responsible of the appearance of a strong ME anisotropy contribution [35,31]. Particularly, size reduction promotes a preferential crystal orientation in NWs grown by electrodeposition into the nanopores of AAO membranes [36,37] and the appearance of residual stress as a consequence of structural confinement [38]. These features then make arrays of Ni NWs good candidates as semihard magnets that combine a low saturation magnetization with high effective anisotropy energies up to $1.4-1.6\times10^{6}$ erg·cm$^{-3}$ ($140-160$ kJ·m$^{-3}$). Therefore, fine tuning of the room temperature magnetic anisotropy enhancement in low diameter Ni NWs is desirable for applications that require control on magnetization reversal, microwave absorption and multiferroic responses. The careful adjustment of electrodeposition conditions is then a key aspect for the fabrication of arrays of Ni NWs with control on their magnetic properties. It has been recently shown that the variation of the deposition potential, in a limited range in order to avoid hydrogen evolution reactions, only slightly modifies the magnetic anisotropy of the Ni NW arrays [31], which means that an alternative strategy has to be followed to change such magnetic property. As suggested in a previous work, changes in the NWs magnetization squareness can be induced by changing the electrolytic bath acidity [39]. However, the magnetization squareness measured from hysteresis loops is a qualitative characterization of the magnetic properties, then a further detailed analysis is needed in order to precisely quantify the influence of electrochemical parameters like the electrolyte pH on the magnetic anisotropy of arrays of Ni NWs.

In this work, we report on the accurate determination by ferromagnetic resonance (FMR) of the effective anisotropy energy of arrays of low diameter (50 nm) Ni NWs into the pores of AAO membranes in which their microstructure has been controlled by adjusting the electrolytic bath acidity. The microstructural analysis carried out by high resolution transmission electron microscopy (HRTEM) observations and X-ray diffraction (XRD) experiments, has revealed a close relation with the magnetic properties of the arrays. In turn, this has led to larger anisotropy energies at higher pH values than the expected magnetostatic anisotropy for arrays of large diameter NWs made of cubic crystal materials like Ni. We also report on the fact that NWs with a preferred crystal texture alone is not a sufficient condition for the enhancement of the magnetic anisotropy. Instead, synthesizing NWs conformed of very large high quality crystals is a necessary condition to improve their magnetic properties. FMR, as a powerful technique, has provided accurate large values of the uniaxial anisotropy energy and hardness parameter, which are in the ranges $64-167$ kJ·m$^{-3}$ and $0.47-0.75$, respectively. This is the first time to our knowledge that distinct and large effective magnetic energies within the semihard magnets region for Ni NWs have been accurately determined and compared to energy values of other materials. Our results then provide a further insight on the possibility of taking advantage of fine tuning unconventional magnetic effects and contributions for the development of more agile technological devices.

## 2. Materials and methods

Arrays of parallel Ni NWs have been synthesized by a standard three-probe electrodeposition technique into the pores of commercial 90 $\mu$m thick AAO membranes from Synkera Technologies, Inc. In this configuration a Pt counter electrode as well as a Ag/AgCl reference electrode have been used. The porosity ($P$) and the pores diameter ($d$) of the AAO membranes are 12 % and 50 nm, respectively. The membrane porosity corresponds to the NWs packing fraction provided that the very good pores filling after electrodeposition is performed. A Cr/Au bilayer, with respective Cr and Au layers thicknesses of 20 nm and 600 nm, has been evaporated onto one side of the membranes to serve as cathode for the electrodeposition and as ground plane for the FMR experiments. Electrolytes with composition 262.8 g l$^{-1}$ $NiSO_4$ + 30 g l$^{-1}$ $H_3BO_3$, but with the pH previously adjusted to the different values 1.6, 2.6, 3.2 and 5.0, have been used for the growth of Ni NWs. Electrolyte pH adjustment has been performed using a VWR pHenomenal benchtop pH meter. The as-prepared electrolytes have pH = 3.8, which has been adjusted to lower and higher values by the addition of $H_2SO_4$ and NaOH, respectively. Electrodeposition has been done in the potentiostatic mode at room temperature by applying a constant potential of −1.05 V. Control on the deposition time has allowed to grow Ni NWs with two different lengths ($h$) of about $13.5\pm0.5$ $\mu$m and $72.0\pm0.5$ $\mu$m, which has been confirmed by following an optical microscopy procedure from the cross section of the AAO membranes containing the NWs, as reported previously [35]. After dissolution of the samples by sonication in concentrated NaOH (1.0 M) to obtain dispersed NWs, HRTEM observations have been carried out using a Jeol JEM-ARM200F atomic resolution analytical electron microscope in order to characterize the crystallite size and orientation in the different NW samples. Complementary structural characterization of the NWs has been done by XRD experiments using a Bruker D2 Phaser X-ray diffractometer with a Cu radiation source of wavelength $\lambda = 1.54$ Å. Room temperature FMR and alternating gradient magnetometry (AGM) measurements have been performed for the determination of the magnetic anisotropy of NW arrays. FMR experiments have been carried out in the saturated state using the microstrip transmission line method and absorption spectra have been recorded in the field swept mode with the applied DC field in the direction of the NWs axis in the range from 10 kOe down to zero field. Hysteresis loop measurements have been recorded in the range ±10 kOe with the magnetic field applied in the directions parallel and perpendicular to the NWs.

## 3. Results and discussion

The evidence of the influence of the electrolytic bath acidity on the microstructure of 72 $\mu$m long Ni NWs deposited in AAO membranes is provided by XRD experiments. Fig. 1 shows diffraction patterns for Ni NWs synthesized at the pH values of 1.6, 3.2 and 5.0. All patterns are similar as they show a preferential (220) texture. However, the difference between them is the presence of small diffraction peaks for the (111), (200) and (311) crystal planes for the NW array synthesized at the lowest pH. Arrays of NWs synthesized at the intermediate pH values also show a strong (220) texture. These results show that the electrolyte pH has a little effect only at very low values, which can be ascribed to the very long length of the NWs that promotes the strong (220) texture, as suggested by previous works [35,40]. Besides, HRTEM characterization has been carried out to gain a better insight on the microstructure of the

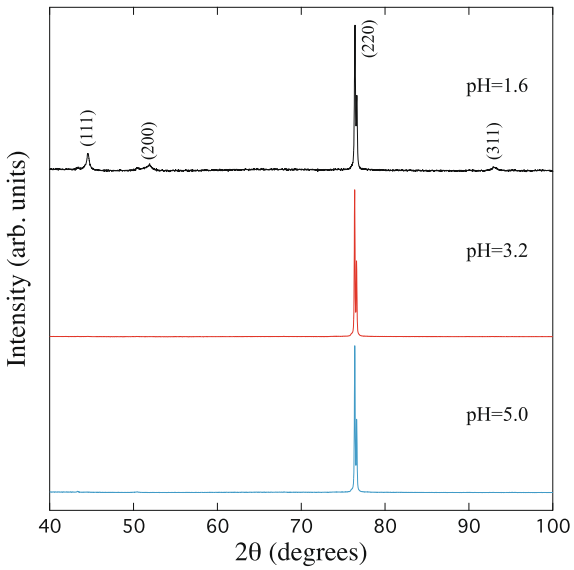


**Fig. 1.** XRD patterns of arrays of 50 nm diameter Ni NWs synthesized using electrolytic baths at pH values of 1.6, 3.2 and 5.0. The patterns are vertically offset for comparison and a legend for each crystal plane is indicated besides its corresponding diffraction peak.

NWs. For this purpose, three samples of dispersed 72 $\mu$m long NWs obtained by dissolution of arrays of NWs fabricated at pH values of 1.6, 3.2 and 5.0 have been analyzed. Figs. 2(a), (b) and (c) display low magnification TEM micrographs of representative sections of Ni NWs synthesized at each pH value. As expected, the electrolytic bath acidity during the fabrication process has a significant impact on the microstructure of the NWs, where the very polycrystalline microstructure at low pH values can be explained by the hydrogen absorption and evolution during the electrodeposition process [41]. By comparing these micrographs, two main features can be observed: the change of both the degree of polycrystallinity and the crystallite size. Particularly, Ni NWs fabricated at pH 1.6 are very polycrystalline with average crystallite size of about $18 \pm 15$ nm. Fig. 2(a) reveals small crystals with non elongated shapes. A more detailed statistical analysis reveals the presence of the crystalline planes (111), (200) and (220) in the same NW, with preferential (111) texture and corresponding volumetric fraction of about 68%. As seen in the HRTEM micrograph of Fig. 2(d) corresponding to a small portion of the NW shown in Fig. 2(a), the dislocations indicated by the dashed lines reveal several small crystals randomly oriented. Other crystals with distinct plane orientations occupy lower volumetric fractions, as for instance, about 20% for the (200) planes. As observed in Fig. 2(b), Ni NWs synthesized at the intermediate pH 3.2 are composed of larger crystals than those for the pH 1.6 sample, with preferential orientation along the [110] direction. The dislocations indicated by the dashed lines in Fig. 2(e) clearly define the boundaries between crystals, which are well defined in contrast to what is observed for the pH 1.6 sample in Fig. 2(d). Furthermore, twinned (220) crystals are clearly evidenced in Fig. 2(e). In this case, the size of the smaller crystals is about $22 \pm 18$ nm, whereas the elongated crystals have a width of about the NWs diameter and a length slightly larger than 100 nm, as seen in Fig. 2(b). For this pH value, preferential (220) planes with volumetric fraction of about 47% are accompanied with (111) planes with lower volumetric fraction of about 41%. The (200) crystal orientation has also been observed, however its volumetric fraction is lower than those for the (220) and (111) planes. Increasing further the pH up to 5.0 leads to very large crystallites oriented along the [110] direction with the same width as the NWs diameter and a length larger than 100 nm, as seen in Fig. 2(c). The corresponding HRTEM micrograph displayed in Fig. 2(f) corroborates an orientation along the [110] direction, which is nearly parallel to the NWs axis. The inset at the low corner in this figure displays a close view of the same image which clearly shows the (220) texture at a direction close to the NW axis. These results are consistent with the fact that absorption of stable hydrolyzed species results in a stable growth at larger pH values [41]. Although at this pH value very large crystals are predominant, polycrystalline non-textured sections, mostly at the base of the NWs where the growth begins, have been observed as well. In this case only the (220), (111) and (200) crystal planes have been observed, with corresponding volumetric fractions of about 61%, 29% and 10%, respectively. In the TEM statistical analysis, the non negligible percentage of (111) planes arise from the polycrystalline sections of the NWs at their initial growth stage. Therefore, the crystallites volumetric fractions are representative of the observed

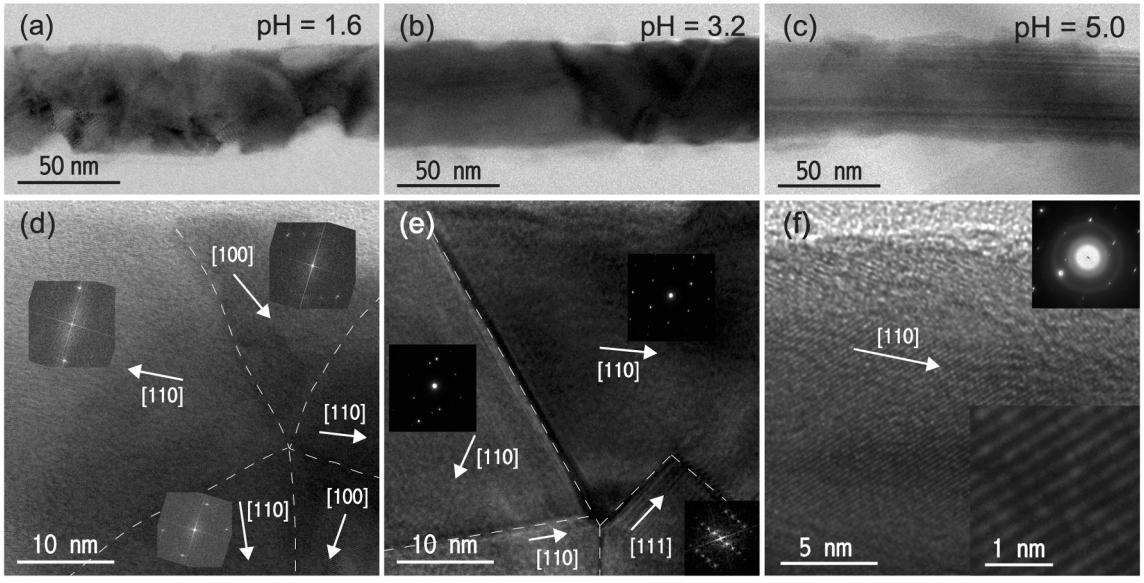


**Fig. 2.** Low magnification bright field TEM micrographs for 50 nm diameter and 72 $\mu$m long Ni NWs synthesized from electrolytic baths with its pH adjusted to (a) 1.6, (b) 3.2. and (c) 5.0. High resolution TEM micrographs for small portions of Ni NWs synthesized at pH of (d) 1.6, (e) 3.2. and (f) 5.0. The direction of the NWs axis is, as in (a), (b) and (c), along the horizontal orientation. The insets in these figures show electron diffraction patterns obtained from the selected sections separated by dashed lines which serve as guides for the eye. The inset at the bottom-right corner in (f) is a close view of the atomic arrangement of the crystal.

NWs, so they do not provide the overall information given by the XRD diffraction patterns. In contrast to the results obtained by XRD that suggest a strong (220) texture regardless the pH of the electrolytic bath, HRTEM provide more accurate information about the NWs microstructure and crystallite size as it allows to locally analyze specific sections of the NWs. Another interesting feature observed in Figs. 2(a)–(c) is the different NWs surface roughness which is very probably induced during the sonication dissolution process. Indeed, by comparing these figures, it is observed that the surface roughness is reduced as the pH is increased, indicating that crystallites of lower sizes are removed at larger pH values. Therefore, NWs embedded in AAO membranes are expected to have negligible roughness in comparison to that of the NWs shown in Fig. 2.

The microstructural changes observed in Figs. 1 and 2 have a significant impact on the magnetic behavior of Ni NW fabricated using electrolytic baths with different acidities as seen in Figs. 3(a) and (b). These figures show FMR absorption spectra recorded at 27 GHz for arrays of short ($h = 13$ $\mu$m) and long ($h = 72$ $\mu$m) Ni NWs synthesized at pH values of 1.6 (dashed lines), 2.6 (dashed-dotted lines), 3.2 (dotted lines) and 5.0 (continuous lines). The resonance field ($H_r$) corresponds to the field value at the minimum of the absorption spectra which provides a direct insight of the effective anisotropy field ($H_{eff}$). For arrays of parallel NWs with the external direct current (DC) magnetic field applied along their axis, the FMR condition is given by

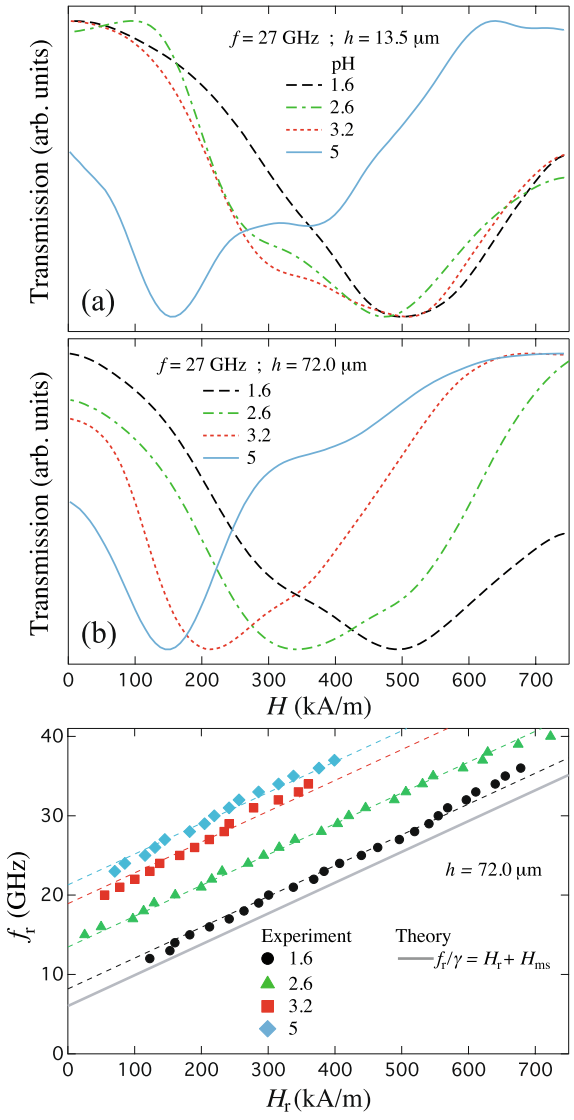


**Fig. 3.** FMR absorption spectra recorded at 27 GHz for arrays of 50 nm diameter Ni NWs synthesized using electrolytic baths at different pH values and with length of (a) 13.5 $\mu$m and (b) 72.0 $\mu$m. (c) Dispersion relations (symbols) for the samples in (b) and linear fits (dashed lines) using Eq. (1). The continuous grey line is calculated using Eqs. (1) and (2) with $H_{eff} = H_{ms}$, so it corresponds to the dispersion relation of a purely MS array of Ni NWs.

$$\frac{f_r}{\gamma} = H_r + H_{eff}, \tag{1}$$

where $f_r$ is the resonance frequency and $\gamma = 3.09$ GHz/kOe is the gyromagnetic ratio for Ni [42]. As seen in Figs. 3(a) and (b), there is a clear variation of $H_r$ at constant frequency with the electrolytic bath acidity for short and long Ni NWs. According to Eq. (1), such a variation is the same for $H_{eff}$ as long as $f_r$ remains constant, leading a maximum field difference of about 5 kOe between the anisotropy field values for samples synthesized at the lower and larger pH. These results are consistent with previous works which have shown that the modification of the electrolyte acidity has a direct influence on the microstructure and magnetic properties of Co and Ni thin films [43,44] and NWs [45–49]. As a result, the magnetic anisotropy of polycrystalline NWs can not include contributions from the crystal structure, so the only magnetic contribution is due to the magnetostatic (MS) or shape anisotropy field [45]. It is then expected that the magnetic anisotropy of polycrystalline low diameter Ni NWs is mainly MS. Indeed, for arrays of NWs synthesized using the most acid electrolytic bath (pH 1.6) the resonance field is close to the expected value considering that $H_{eff}$ is given by the MS field

$$H_{ms} = \frac{1}{2}M_s(1 - 3P), \tag{2}$$

where $P = 0.12$ and $M_s = 485$ kA·m$^{-1}$ are the packing fraction of the NWs in the AAO membranes and the saturation magnetization of Ni, respectively [42]. Using these values along with Eqs. (1) and (2) lead to $H_{ms} = 155.2$ kA·m$^{-1}$ and $H_r = 540.3$ kA·m$^{-1}$, where this last value is close to the resonance field for both arrays of short and long Ni NWs synthesized at pH = 1.6 (see Figs. 3(a) and (b)).

On the other hand, comparing the absorption spectra for arrays of short and long Ni NWs reveal important differences that deserve to be discussed. First, the most of the spectra display a complex lineshape as they are composed of a main absorption peak accompanied by a secondary shoulder-like absorption [35]. As pointed out previously, these absorptions are the fingerprint of the two growth stages of Ni NWs in AAO membranes that consist of a polycrystalline stage followed by a single crystalline one. Since the effective anisotropy field of the single crystalline stage is larger than that of the polycrystalline one, then their corresponding resonance fields take place respectively at lower and larger values, as suggested by Eq. (1). Therefore, as seen in Fig. 3(a), the main FMR absorption for arrays of short Ni NWs grown from acidic electrolytic baths (pH $\leqslant$3.2) arises from the polycrystalline stage, as expected. However, the depth of the shoulder in the absorption spectra observed at lower resonance fields increases as the pH increases. This feature is consistent with a change in the microstructure of the NWs, so that they are less polycrystalline and larger crystals are present as shown in Fig. 2. As the pH is further increased to 5.0, the main absorption is consistent with a microstructure composed of large single crystals with (220) texture, *i.e.*, they are no longer mainly polycrystalline. In this case, even if the NWs are not too long their magnetic anisotropy is larger than that for very polycrystalline Ni NWs (pH close to 1.6) given by Eq. (2). Therefore, $H_{eff}$ corresponds to the superposition of the MS field and an additional field, which has been proven to be of magnetoelastic (ME) origin [31,35], that is

$$H_{eff} = H_{ms} + H_{me}, \tag{3}$$

where $H_{me}$ is the additional ME field which has been related to residual stresses on NWs due to their confined growth inside the pores of the AAO membranes. This effect combined with the non-negligible magneto-

striction of Ni are responsible of the appearance of the significant ME anisotropy contribution. Indeed, a proof of the ME nature of this contribution is provided by the fact that arrays of Py ($Ni_{80}Fe_{20}$) NWs with no magnetostriction confined in the same porous matrixes do not show any additional anisotropy contribution [35].

Besides, the absorption spectra for arrays of very long Ni NWs ($h = 72\ \mu$m) shown in Fig. 3(b) also display the complex lineshape as that for short NWs. However, in this case the dominant FMR absorption takes place at lower resonance fields for most of the samples, in contrast to what is observed in Fig. 3(a). This scenario is consistent with a two stage growth for which the polycrystalline segment, that takes place at the first growth stage, has a limiting length along the NWs. As a result, the corresponding FMR absorption displayed as a shoulder at higher resonance fields has lower intensity with respect to the main absorption peak, that corresponds to the preferred and longer single crystalline growth at the second stage. That is, this single crystal growth is responsible of the dominant FMR absorption peak in the spectra for Ni NWs synthesized at pH $\geqslant$2.6. Conversely, the main FMR absorption located at higher resonance fields for the array of Ni NWs synthesized at pH = 1.6 indicates that even when the NWs are very long their microstructure is mainly polycrystalline. Besides, from Fig. 3(a) it is observed that $H_r$ is almost the same for samples synthesized at pH $\leqslant$3.2, but a sudden field shift takes place when the pH increases up to 5.0. In contrast, a progressive resonance field shift towards lower values is observed for long NWs as the pH increases (see Fig. 3(b)). Therefore, a more accurate control of the magnetic anisotropy as a function of the electrolytic bath acidity can be achieved with longer Ni NWs rather than with shorter ones. With this consideration, a complete characterization of the FMR response of each array of long Ni NWs deposited at different pH values can be obtained from the dispersion relations. As shown in Fig. 3(c), these type of measurements for each sample with long NWs are carried out by recording absorption spectra at different resonance frequencies in the range from 10 GHz to 40 GHz. From this figure it is clear that reducing the electrolytic bath acidity leads to an increase of the resonance frequency at a fixed resonance field, which is accompanied with an increase of $H_{eff}$. This field can then easily be determined by using Eq. (1) as fitting function to the experimental dispersion relations, shown as dotted lines in Fig. 3(c). The theoretical dispersion relation for an array of Ni NWs with only MS anisotropy contributions can be determined by combining Eqs. Eq 1 and 2 and taking $H_{eff} = H_{ms}$ (see the continuous grey line). As observed, this curve lies below all the dispersion relations, thus showing that it corresponds to a lower bound for the magnetic anisotropy of the arrays of Ni NWs considered in this study. It must be stressed that the array of NWs with the higher polycrystallinity and synthesized from the most acid solution is very close to this lower bound. This feature corroborates the dominant MS behavior for this sample and the presence of an additional anisotropy contribution for the other samples. Besides, since the surface roughness of NWs embedded in AAO membranes is expected to be very low, no magnetic contributions arising from this feature are considered in Eq. (3). Otherwise, this would result in reduced $H_{eff}$ values, even lower than $H_{ms}$, as a result of significant opposing magnetostatic contributions arising from surface pits, which is contrary to what is observed in Fig. 3(c) since all dispersion relations lie above the grey line.

On the other hand, hysteresis loops recorded with the magnetic field applied along the directions parallel and perpendicular to the NWs provide additional information about their magnetic anisotropy. Short and long Ni NWs have been characterized by AGM in order to better understand the influence of electrochemical growth conditions on both their microstructure and magnetic properties. For short Ni NWs ($h \approx 13.5\ \mu$m) the increase of the remanence ($M_r = M(0)/M_s$) with the pH observed from the hysteresis loops recorded with the field parallel to the NWs axis indicates a reinforcement of the magnetization easy axis along the NWs (see Fig. 4(a)). Moreover, the larger saturation field $H_s$ at pH = 5.0 observed from the hysteresis loops recorded in the direction perpendicular to the NWs axis (see Fig. 4(b)), corroborates the

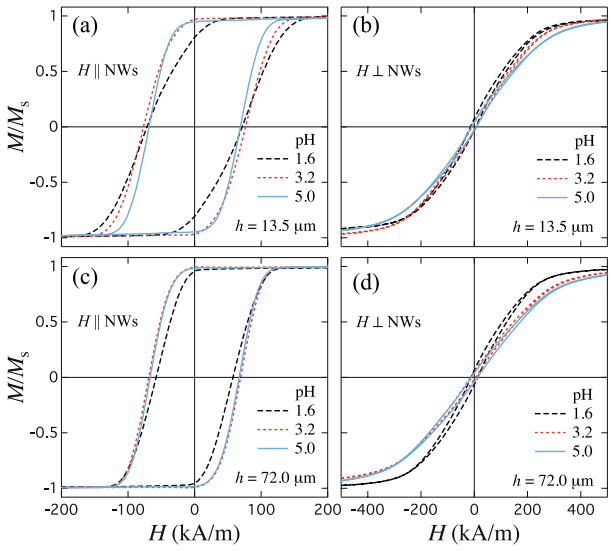


**Fig. 4.** Hysteresis loops recorded for arrays of 50 nm diameter Ni NWs deposited at pH values of 1.6, 3.2 and 5.0. Measurements done for 13.5 $\mu$m long NWs with the applied field (a) parallel to its axis and (b) perpendicular to its axis. Measurements done for 72.0 $\mu$m long NWs with the applied field (c) parallel to its axis and (d) perpendicular to its axis.

reinforcement of the magnetic anisotropy along the NWs axis at larger pH values. Since the growth mechanism of low diameter Ni NWs in AAO membranes proceeds via an initial polycrystalline segment followed by a single-crystalline segment [35,36,40], short Ni NWs grown under standard conditions (pH $\approx$ 3.8) are expected to be mainly polycrystalline. Conversely, the largest saturation field obtained for the pH 5.0 NW array suggest that the microstructure of Ni NWs deposited at pH 5.0 must be preferably single-crystalline despite its short length, which is consistent with the results shown in Fig. 3(a). Besides, larger $M_r$ and $H_s$ values are also obtained with increasing the electrolyte pH for longer NWs, as seen from the hysteresis loops measured respectively in the directions parallel and perpendicular to the NWs axis (see Figs. 4(c) and (d)). Values of the coercive field ($H_c$), saturation field ($H_s$) and remanence ($M_r$) for arrays of short and long Ni NWs measured with the magnetic field applied in the directions parallel (||) and perpendicular ($\perp$) to the NWs are summarized in Table 1. Besides, Table 1 also includes the squareness of the hysteresis loops from measurements carried out with the field applied along the NWs axis, which reads

$$S = \frac{1}{H_c M_r}\int_{-H_c}^{0} M(H)dH. \tag{4}$$

**Table 1**
Values of the coercive field ($H_c$), saturation field ($H_s$) and remanence ($M_r$) for arrays of Ni NWs with lengths $h = 13.5\ \mu$m and $h = 72.0\ \mu$m measured with the magnetic field applied in the directions parallel (||) and perpendicular ($\perp$) to their axis. The hysteresis loops squareness $S$ is obtained using Eq. (4) with the field applied along the NWs axis. Saturation and coercive fields units are in kA·m$^{-1}$.

| pH | $H_c^{\parallel}$ | $H_s^{\parallel}$ | $M_r^{\parallel}$ | $S$ | $H_c^{\perp}$ | $H_s^{\perp}$ | $M_r^{\perp}$ |
|---|---|---|---|---|---|---|---|
| *Short nanowires ($h = 13.5\ \mu m$)* | | | | | | | |
| 1.6 | 71.986 | 192.562 | 0.807 | 0.556 | 14.117 | 837.036 | 0.071 |
| 3.2 | 78.241 | 227.926 | 0.969 | 0.658 | 8.364 | 675.916 | 0.036 |
| 5.0 | 68.930 | 340.910 | 0.947 | 0.721 | 10.456 | 880.263 | 0.042 |
| *Long nanowires ($h = 72.0\ \mu m$)* | | | | | | | |
| 1.6 | 58.163 | 196.382 | 0.955 | 0.615 | 8.364 | 682.807 | 0.036 |
| 3.2 | 69.734 | 131.359 | 0.993 | 0.704 | 14.332 | 958.424 | 0.050 |
| 5.0 | 66.988 | 248.545 | 0.984 | 0.715 | 10.051 | 960.909 | 0.037 |

The integral in the numerator corresponds to the area of the second quadrant of the hysteresis loop [50]. This parameter has an upper bound of 1 and provides a measure of the rectangularity of the hysteresis loop which is proportional to the effective magnetic anisotropy according to the Stoner–Wohlfarth model. Although the coercive field is almost unchanged, the monotonous increase of $S$ with the pH for both arrays of short and long NWs is in good agreement with the increase of the magnetic anisotropy obtained by the FMR experiments. As seen, long Ni NWs display both squarer hysteresis loops in the direction parallel to the NWs and larger saturation fields in the direction perpendicular to the NWs, in contrast with short NWs synthesized at the same electrolyte pH. The increase of these parameters for longer NWs indicates an improvement of the crystal quality and texture along the [110] direction as their growth continue regardless their pH value. The crossover between conditions that favors magnetic anisotropy enhancement is evident from the comparison between Figs. 3 and 4. On the one hand, short Ni NWs are mostly polycrystalline so no anisotropy enhancement is expected unless their growth is done at the highest pH of 5.0, as observed in Fig. 3 (a). On the other hand, long Ni NWs tend to be single cristalline with strong (220) texture showing a clear anisotropy enhancement for NWs grown at all pH values with the exception of those grown at the highly acidic pH of 1.6, as observed in Fig. 3(b).

Although both measurement techniques AGM and FMR provide complementary information about the magnetic behavior of Ni NWs, FMR can provide more quantitative information about the effect of the electrolyte acidity on the precise anisotropy enhancement of the NWs (see Fig. 3). The progressive shift of the resonance field observed in Fig. 3(b) indicates that the fine tuning of the magnetic anisotropy enhancement with the electrolyte pH can only be achieved by considering very long Ni NWs instead of short ones. In this sense, the effective anisotropy field $H_{\text{eff}}$ can be determined by fitting the resonance condition of Eq. (1) to the corresponding FMR dispersion relations shown in Fig. 3(c). Using these $H_{\text{eff}}$ values along with Eq. (3) allows to obtain the ME field $H_{\text{me}}$ and thus the additional uniaxial ME energy given by

$$K_{\text{me}} = \frac{1}{2}\mu_0 M_s H_{\text{me}} = \frac{1}{2}\mu_0 M_s (H_{\text{eff}} - H_{\text{ms}}). \tag{5}$$

In this equation the MS field $H_{\text{ms}} = 155.2\ \text{kA}\cdot\text{m}^{-1}$ for all the samples as indicated above in the text. The additional ME anisotropy obtained using Eq. (5) is plotted in Fig. 5(a) as a function of the electrolyte pH. Error bars of the data in this figure have been obtained from the statistical dispersion of the experimental $f_r$ vs $H_r$ dispersion relations. That is, errors for the ME energy correspond to one standard deviation at 99% confidence interval of the zero field resonance frequency ($f_0$) and are given as $\Delta K_{\text{me}} = \pm\frac{M_s}{2\gamma}\Delta f_0$. As expected, the additional ME energy increases monotonically with increasing the electrolyte pH in the range from 1.6 to 5.0. At the lowest (highest) pH value $K_{\text{me}}$ is equal to 16.9 $\text{kJ}\cdot\text{m}^{-3}$ (120 $\text{kJ}\cdot\text{m}^{-3}$) giving place to a total increase of the ME energy of 103 $\text{kJ}\cdot\text{m}^{-3}$ in this pH range. This value is more than twice the uniaxial magnetostatic energy $K_{\text{ms}} = \frac{1}{2}\mu_0 M_s H_{\text{ms}} = 47.3\ \text{kJ}\cdot\text{m}^{-3}$ and larger by one order of magnitude than the magnetocrystalline (MC) energy $K_{\text{mc}} = \frac{K_1}{4} = -1.3\ \text{kJ}\cdot\text{m}^{-3}$ along the preferred crystal direction [110] for long Ni NWs, where $K_1 = -5\ \text{kJ}\cdot\text{m}^{-3}$ is the first order MC constant of Ni [42].

Comparing the results in Fig. 5(a) with those of Fig. 2, a direct correlation between the magnetic properties and the crystallite size is observed, such that both increase with the electrolyte pH. As a consequence, larger crystallites confined into nanopores of reduced diameter lead to larger anisotropy field values. Besides, given that very long Ni NWs have a similar strong (220) texture regardless the pH value, as seen in Fig. 1, a strong (220) texture is a necessary but not a sufficient condition for the appearance of strong magnetoelastic effects. Specifically, NWs synthesized at pH 1.6 are composed of small crystallites with strong (220) texture, however this condition is not sufficient for the strong ME contribution to be induced. Conversely, this additional anisotropy

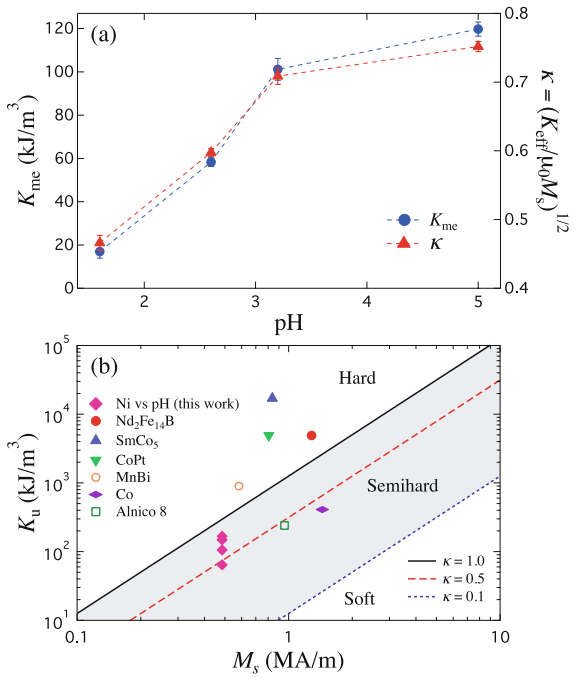


**Fig. 5.** (a) Variation of $K_{\text{me}}$ and $\kappa$ as a function of the electrolyte pH for arrays of 50 nm diameter and 72.0 $\mu$m long Ni NWs embedded in AAO membranes. The dotted line is a guide for the eye and error bars correspond to one standard deviation at 99% confidence interval. (b) Log-plot of the variation of $K_u$ as a function of $M_s$ for some representative rare-earth and rare-earth-free based magnetic materials [51] and the arrays of Ni NWs fabricated at different pH values in this work (lozenges). The anisotropy energy for Ni NWs has been obtained using the expression $K_u = K_{\text{eff}} = K_{\text{ms}} + K_{\text{me}}$. The semihard region highlighted in grey is delimitated by the curves $\kappa = 0.1$ and $\kappa = 1.0$ calculated using the equation $\kappa = \sqrt{K_u/(\mu_0 M_s^2)}$.

contribution is induced in NWs synthesized at pH 5.0 as they fulfill both conditions of a strong (220) texture and very long crystallites. It is worth mentioning that the observed behavior in Fig. 5(a) is not clearly observed for short Ni NWs since the effective energy is preferably dominated by the MS contributions at pH values below 5.0, whereas the ME contribution can be non negligible at this last pH value which gives rise to a sudden increase of the effective anisotropy field. Therefore, a key requirement to observe a monotonous increase of the energy enhancement contribution is a very long length of the NWs.

Besides, the effective anisotropy energy of the NWs given by $K_{\text{eff}} = K_{\text{ms}} + K_{\text{me}}$ is of uniaxial nature and is in the range 64 –167 $\text{kJ}\cdot\text{m}^{-3}$, so it can be used to compute the corresponding hardness parameter for each array. This parameter is defined in terms of the ratio of the uniaxial anisotropy to magnetostatic energy, that is $\kappa = \sqrt{K_u/(\mu_0 M_s^2)}$ [14]. Using Eq. (5) along with the expression for $K_{\text{ms}}$ given above and $K_u = K_{\text{eff}}$ allows writing $\kappa$ as follows

$$\kappa = \left(\frac{1-3P}{4} + \frac{K_{\text{me}}}{\mu_0 M_s^2}\right)^{1/2}. \tag{6}$$

Eq. (6) is useful to determine whether a material is a hard ($\kappa > 1$) or a semihard magnet ($0.1 < \kappa < 1$), provided that $\kappa \gtrsim 0.5$ is required for its potential use as a permanent magnet [13]. The obtained hardness parameter as a function of the electrolyte pH is plotted in Fig. 5(a). The increase of $\kappa$ from 0.47 to 0.75 as the pH increases suggest that arrays of Ni NWs grown at the higher pH values can be used as potential permanent nanomagnets. Conversely, arrays of NWs with both negligible and low $K_{\text{me}}$ values (pH 1.6) lead to $\kappa$ values of 0.40 and 0.47, respectively, so they are not suitable for permanent magnet applications. Error

bars for $\kappa$ correspond to one standard deviation and are obtained from error bars for $K_{\mathrm{me}}$ as $\sigma_\kappa = \sigma_{K_{\mathrm{me}}}/(2\kappa\mu_0 M_s^2)$. Fig. 5(b) shows a log-plot that compares the uniaxial anisotropy as a function of the saturation magnetization for the arrays of Ni NWs fabricated in this work using solutions at different pH values (lozenges) and some representative rare-earth and rare-earth-free based materials lying in both the semihard and hard magnet regions [51]. As seen in the figure, the three regions for soft, semihard and hard magnets are separated by straight lines which are calculated using the equation $\kappa = \sqrt{K_u/(\mu_0 M_s^2)}$. The array of Ni NWs deposited with the most acidic solution as well as the Co and Alnico 8 alloy have $K_u$ values lying just beneath the $\kappa = 0.5$ curve, so these materials represent a lower bound for potential permanent magnet applications. Nevertheless, Ni NWs deposited using less acidic solutions display larger effective uniaxial energies that approach to the upper bound $\kappa = 1$ of semihard magnets. Particularly, the fact that $K_u = 167$ kJ·m$^{-3}$ for the pH 5.0 array of Ni NWs lies close to this bound, but also since it is comparable to the $K_u$ values of Co and Alnico alloys, makes arrays of confined Ni NWs interesting materials for the development of more agile devices based on semihard nanomagnets.

## 4. Conclusions

In this work we have obtained accurate values of the effective uniaxial anisotropy energy by ferromagnetic resonance of arrays of 50 nm diameter Ni NWs in AAO membranes in which their microstructure has been controlled by adjusting the electrolytic bath acidity. This has led to larger anisotropy energies than the expected magnetostatic anisotropy for arrays of larger diameter NWs made of cubic crystal materials like Ni, which is the result of an additional magnetoelastic contribution that progressively increases with the solution pH. The microstructural characterization carried out by XRD and HRTEM measurements have revealed a strong relation between the electrodeposition conditions and the crystal quality of the NWs. Furthermore, we have shown that NWs with a preferred crystal texture alone is not a sufficient condition for the enhancement of the magnetic anisotropy, but rather it is necessary to obtain NWs made of very large high quality crystals. Besides the expected increase of the magnetization squareness with the pH by typical AGM measurements, FMR has provided an accurate and quantitative analysis of the uniaxial anisotropy energy and hardness parameter because it is able to directly extract the effective anisotropy field. Therefore, the control on the electrodeposition conditions allows changing the effective anisotropy energy with the pH in the wide range of 64 –167 kJ·m$^{-3}$. Hardness parameters in the range 0.47–0.75 within the semihard region, have been obtained from these energies. These results suggest that arrays of confined very long and low diameter Ni NWs synthesized using the less acidic electrolytes are interesting for its potential use as permanent nanomagnets. Finally, the possibility of fine tuning unconventional magnetic effects and contributions is a key aspect for the development of tunable and more agile microwave and spintronic devices.

## CRediT authorship contribution statement

**Jonathan Almazán-Celis:** Methodology, Investigation, Validation, Data curation. **Luis E. Díaz-Sánchez:** Investigation, Resources, Validation. **Oscar F. Olea-Mejía:** Validation, Data curation, Formal analysis. **Luc Piraux:** Supervision, Writing - review & editing, Resources, Funding acquisition. **Joaquín de la Torre Medina:** Conceptualization, Supervision, Funding acquisition, Formal analysis, Writing - original draft.

## Declaration of Competing Interest

The authors declare that they have no known competing financial interests or personal relationships that could have appeared to influence the work reported in this paper.

## Acknowledgements

This work was partly supported by the Fédération Wallonie-Bruxelles (ARC 18/23-093 MICROBAT) and by the Fonds de la Recherche Scientifique-FNRS under Grant No. T.0006.16 and by the CONACYT project A1-S-9588 and the 2019 UNAM-DGAPA-PAPIIT Program project IN106619. L. E. D.-S. and J. A.-C. want to thank CONACYT for financial support through project 182290. The authors would like to thank Josué E. Romero Ibarra (IIM-UNAM) for his technical assistance with the TEM measurements.

## References

[1] Sabpreet Bhatti, Rachid Sbiaa, Atsufumi Hirohata, Hideo Ohno, Shunsuke Fukami, S.N. Piramanayagam, Spintronics based random access memory: a review, Materials Today 20 (9) (2017) 530–548.
[2] Gerrit E.W. Bauer, Eiji Saitoh, Bart J. van Wees, Spin caloritronics, Nature Materials 11 (5) (2012) 391–399.
[3] Xichao Zhang, Yan Zhou, Kyung Mee Song, Tae-Eon Park, Jing Xia, Motohiko Ezawa, Xiaoxi Liu, Weisheng Zhao, Guoping Zhao, Seonghoon Woo, Skyrmion-electronics: writing, deleting, reading and processing magnetic skyrmions toward spintronic applications, Journal of Physics: Condensed Matter 32 (14) (2020) 143001.
[4] Stefan Slesazeck, Thomas Mikolajick, Nanoscale resistive switching memory devices: a review, Nanotechnology 30 (35) (Jun 2019), 352003.
[5] Flavio Abreu Araujo, Mathieu Riou, Jacob Torrejon, Sumito Tsunegi, Damien Querlioz, Kay Yakushiji, Akio Fukushima, Hitoshi Kubota, Shinji Yuasa, Mark D. Stiles, Julie Grollier, Role of non-linear data processing on speech recognition task in the framework of reservoir computing, Scientific Reports 10 (1) (2020) 328.
[6] S.X. Wang, G. Li, Advances in giant magnetoresistance biosensors with magnetic nanoparticle tags: Review and outlook, IEEE Transactions on Magnetics 44 (7) (July 2008) 1687–1702.
[7] Frederico R. Baptista, S.A. Belhout, S. Giordani, S.J. Quinn, Recent developments in carbon nanomaterial sensors, Chemical Society Reviews 44 (2015) 4433–4453.
[8] Giovanni Finocchio, Felix Büttner, Riccardo Tomasello, Mario Carpentieri, Mathias Kläui, Magnetic skyrmions: from fundamental to applications, Journal of Physics D: Applied Physics 49 (42) (Sep 2016), 423001.
[9] Catalina E. Carreón-González, Joaquín De La Torre Medina, Luc Piraux, Armando Encinas, Electrodeposition growth of nanowire arrays with height gradient profiles for microwave device applications, Nano Letters 11 (5) (May 2011) 2023–2027.
[10] D. Weller, A. Moser, L. Folks, M.E. Best, Wen Lee, M.F. Toney, M. Schwickert, J.U. Thiele, M.F. Doerner, High $K_u$ materials approach to 100 Gbits/in$^2$, IEEE Transactions on Magnetics 36 (1) (2000) 10–15.
[11] Till Burkert, Lars Nordström, Olle Eriksson, Olle Heinonen, Giant magnetic anisotropy in tetragonal FeCo alloys, Physical Review Letters 93 (Jul 2004), 027203.
[12] S. Okamoto, N. Kikuchi, O. Kitakami, T. Miyazaki, Y. Shimada, K. Fukamichi, Chemical-order-dependent magnetic anisotropy and exchange stiffness constant of FePt (001) epitaxial films, Physical Review B 66 (Jul 2002), 024413.
[13] J.M.D. Coey, Hard magnetic materials: A perspective, IEEE Transactions on Magnetics 47 (12) (Dec 2011) 4671–4681.
[14] J.M.D. Coey, Perspective and prospects for rare earth permanent magnets, Engineering (2019).
[15] Jeotikanta Mohapatra, Meiying Xing, Jacob Elkins, J. Ping Liu, Hard and semi-hard magnetic materials based on cobalt and cobalt alloys, Journal of Alloys and Compounds 824 (2020), 153874.
[16] Aaron Gilad Kusne, Tieren Gao, Apurva Mehta, Liqin Ke, Manh Cuong Nguyen, Kai-Ming Ho, Vladimir Antropov, Cai-Zhuang Wang, Matthew J. Kramer, Christian Long, Ichiro Takeuchi, On-the-fly machine-learning for high-throughput experiments: search for rare-earth-free permanent magnets, Scientific Reports 4 (1) (2014) 6367.
[17] Samuel J. Kernion, R. Paul, Jane Grossmann Ohodnicki, Alex Leary, Shen Shen, Vladimir Keylin, Joseph F. Huth, John Horwath, Matthew S. Lucas, Michael E. McHenry, Giant induced magnetic anisotropy in strain annealed Co-based nanocomposite alloys, Applied Physics Letters 101 (10) (2012), 102408.
[18] Laura H. Lewis, Félix Jiménez-Villacorta, Perspectives on permanent magnetic materials for energy conversion and power generation, Metallurgical and Materials Transactions A 44 (1) (2013) 2–20.
[19] Aleksander L. Wysocki, Manh Cuong Nguyen, Cai-Zhuang Wang, Kai-Ming Ho, Andrey V. Postnikov, Vladimir P. Antropov, Concentration-tuned tetragonal strain in alloys: Application to magnetic anisotropy of $FeNi_{1-x}Co_x$, Physical Review B 100 (Sep 2019), 104429.
[20] Ajaya K. Nayak, Michael Nicklas, Stanislav Chadov, Panchanana Khuntia, Chandra Shekhar, Adel Kalache, Michael Baenitz, Yurii Skourski, Veerendra K. Guduru, Alessandro Puri, Uli Zeitler, J.M.D. Coey, Claudia Felser, Design of compensated ferrimagnetic Heusler alloys for giant tunable exchange bias, Nature Materials 14 (7) (2015) 679–684.
[21] B. Balamurugan, B. Das, V.R. Shah, R. Skomski, X.Z. Li, D.J. Sellmyer, Assembly of uniaxially aligned rare-earth-free nanomagnets, Applied Physics Letters 101 (12) (2012), 122407.

[22] L.H. Lewis, A. Mubarok, E. Poirier, N. Bordeaux, P. Manchanda, A. Kashyap, R. Skomski, J. Goldstein, F.E. Pinkerton, R.K. Mishra, R.C. Kubic Jr, K. Barmak, Inspired by nature: investigating tetrataenite for permanent magnet applications, Journal of Physics: Condensed Matter 26 (6) (2014), 064213.
[23] Koichi Tsuchiya, Akira Ohashi, Daigo Ohtoyo, Hiroyuki Nakayama, Minoru Umemoto, Paul G. McCormick, Phase transformations and magnetostriction in Ni-Mn-Ga ferromagnetic shape memory alloys, Materials Transactions, JIM 41 (8) (2000) 938–942.
[24] M. Weiler, A. Brandlmaier, S. Geprägs, M. Althammer, M. Opel, C. Bihler, H. Huebl, M.S. Brandt, R. Gross, S.T.B. Goennenwein, Voltage controlled inversion of magnetic anisotropy in a ferromagnetic thin film at room temperature, New Journal of Physics 11 (1) (Jan 2009), 013021.
[25] Michal Staňo, Olivier Fruchart, Chapter 3 - magnetic nanowires and nanotubes, in: Ekkes Brück (Ed.), Handbook of Magnetic Materials, volume 27 of Handbook of Magnetic Materials, Elsevier, 2018, pp. 155–267.
[26] Luc Piraux, Magnetic nanowires, Applied Sciences 10 (5) (2020) 1832.
[27] Luc Piraux, Gaël Hamoir, Armando Encinas, Joaquin De La Torre Medina, Flavio Abreu Araujo, Influence of the packing fraction and host matrix on the magnetoelastic anisotropy in Ni nanowire composite arrays, Journal of Applied Physics 114 (12) (2013) 123907.
[28] A. Kumar, S. Fähler, H. Schlörb, K. Leistner, L. Schultz, Competition between shape anisotropy and magnetoelastic anisotropy in Ni nanowires electrodeposited within alumina templates, Physical Review B 73 (Feb 2006), 064421.
[29] Xue Wei Wang, Guang Tao Fei, Xi Jin Xu, Zhen Jin, Li De Zhang, Size-dependent orientation growth of large-area ordered Ni nanowire arrays, The Journal of Physical Chemistry B 109 (51) (2005) 24326–24330.
[30] S. Karim, K. Maaz, Magnetic behavior of arrays of nickel nanowires: Effect of microstructure and aspect ratio, Materials Chemistry and Physics 130 (3) (2011) 1103–1108.
[31] Y. Velázquez-Galván, J. de la Torre Medina, L. Piraux, A. Encinas, Robustness of the enhanced magnetic anisotropy in Ni nanowires regardless of the deposition potential, Journal of Magnetism and Magnetic Materials (2019) 165992.
[32] S. Dubois, J. Colin, J.L. Duvail, L. Piraux, Evidence for strong magnetoelastic effects in ni nanowires embedded in polycarbonate membranes, Physical Review B 61 (Jun 2000) 14315–14318.
[33] Joaquín De La Torre Medina, Michaël Darques, Luc Piraux, Strong low temperature magnetoelastic effects in template grown Ni nanowires, Journal of Physics D: Applied Physics 41 (3) (Jan 2008), 032008.
[34] L. Forzani, A.M. Gennaro, R.R. Koropecki, C.A. Ramos, Sensing anisotropic stresses with ferromagnetic nanowires, Applied Physics Letters 116 (1) (2020), 013104.
[35] J. de la Torre Medina, G. Hamoir, Y. Velázquez-Galván, S. Pouget, H. Okuno, L. Vila, A. Encinas, L. Piraux, Large magnetic anisotropy enhancement in size controlled Ni nanowires electrodeposited into nanoporous alumina templates, Nanotechnology 27 (14) (2016), 145702.
[36] X.H. Huang, G.H. Li, G.Z. Sun, X.C. Dou, L. Li, L.X. Zheng, Initial growth of single-crystalline nanowires: From 3D nucleation to 2D growth, Nanoscale Research Letters 5 (6) (2010) 1057.
[37] Gary S. Harlow, Jakub Drnec, Tim Wiegmann, Weronica Lipé, Jonas Evertsson, Axel R. Persson, Reine Wallenberg, Edvin Lundgren, Nikolay A. Vinogradov, Observing growth under confinement: Sn nanopillars in porous alumina templates, Nanoscale Advances 1 (2019) 4764–4771.
[38] Ho Sun Shin, Jin Yu, Jae Yong Song, Hyun Min Park, Yong-Sung Kim, Origins of size-dependent lattice dilatation in tetragonal Sn nanowires: Surface stress and growth stress, Applied Physics Letters 97 (13) (2010) 131903.
[39] Jun Zhang, YaXin Jin, HanBin Wang, Cong Ye, WeiMing Tong, Hao Wang, Growth and magnetic properties of single crystalline ni nanowire arrays prepared by pulse dc electrodeposition, Science China Physics, Mechanics and Astronomy 54 (7) (2011) 1244–1248.
[40] S. Dellis, A. Christoulaki, N. Spiliopoulos, D.L. Anastassopoulos, A.A. Vradis, Electrochemical synthesis of large diameter monocrystalline nickel nanowires in porous alumina membranes, Journal of Applied Physics 114 (16) (2013), 164308.
[41] A. Vicenzo, P.L. Cavallotti, Growth modes of electrodeposited cobalt, Electrochimica Acta 49 (24) (2004) 4079–4089.
[42] B.D. Cullity, C.D. Graham, Introduction to Magnetic Materials, John Wiley & Sons Inc, 2nd ed. (2009).
[43] Tu. Chen, P. Cavallotti, Electroplated cobalt film for perpendicular magnetic recording medium, Applied Physics Letters 41 (2) (1982) 205–207.
[44] Mustapha Boubatra, Amor Azizi, Guy Schmerber, Aziz Dinia, The influence of ph electrolyte on the electrochemical deposition and properties of nickel thin films, Ionics 18 (4) (2012) 425–432.
[45] Michael Darques, Armando Encinas, Laurent Vila, Luc Piraux, Controlled changes in the microstructure and magnetic anisotropy in arrays of electrodeposited Co nanowires induced by the solution pH, Journal of Physics D: Applied Physics 37 (10) (2004) 1411.
[46] I.Z Rahman, K.M Razeeb, M.A Rahman, Md Kamruzzaman, Fabrication and characterization of nickel nanowires deposited on metal substrate, Journal of Magnetism and Magnetic Materials 262 (1) (2003) 166–169. Proceedings of the International Workshop on Electronics Transport in Magnetic Nanogranular Systems.
[47] Andrea Cortés, Gonzalo Riveros, Juan L. Palma, Juliano C. Denardin, Ricardo E. Marotti, Enrique A. Dalchiele, Humberto Gómez, Single-crystal growth of nickel nanowires: Influence of deposition conditions on structural and magnetic properties, Journal of Nanoscience and Nanotechnology 9 (3) (2009) 1992–2000.
[48] Ji Ung Cho, Jun-Hua Wu, Ji Hyun Min, Seung Pil Ko, Joon Young Soh, Qun Xian Liu, Young Keun Kim, Control of magnetic anisotropy of co nanowires, Journal of Magnetism and Magnetic Materials 303(2) (2006) e281–e285. The 6th International Symposium on Physics of Magnetic Materials.
[49] L.G. Vivas, J. Escrig, D.G. Trabada, G.A. Badini-Confalonieri, M. Vázquez, Magnetic anisotropy in ordered textured co nanowires, Applied Physics Letters 100 (25) (2012), 252405.
[50] Marcos F. de Campos, A. Fernanda, Sampaio da Silva, Elio A. Perigo, José A. de Castro, Stoner–wohlfarth model for the anisotropic case, Journal of Magnetism and Magnetic Materials 345 (2013) 147–152.
[51] R. Skomski, J.M.D. Coey, Magnetic anisotropy — how much is enough for a permanent magnet? Scripta Materialia 112 (2016) 3–8.